Characterizing image quality in a scanning laser ophthalmoscope with differing pinholes and induced scattered light

Jennifer J. Hunter*

Department of Physics and Astronomy and School of Optometry, University of Waterloo, and Guelph-Waterloo Physics Institute, Waterloo, Canada N2L 3G1

Christopher J. Cookson

Department of Physics and Astronomy, University of Waterloo, Canada N2L 3G1

Marsha L. Kisilak

Department of Physics and Astronomy and School of Optometry, University of Waterloo, Canada N2L 3G1

Juan M. Bueno

Laboratorio de Óptica, Centro de Investigación en Óptica y Nanofisica, Universidad de Murcia, Campus de Espinardo, 30071 Murcia, Spain

Melanie C. W. Campbell

Department of Physics and Astronomy and School of Optometry, University of Waterloo, and Guelph-Waterloo Physics Institute, Waterloo, Canada N2L 3G1

Received August 22, 2006; revised November 2, 2006; accepted November 6, 2006; published April 11, 2007

We quantify the effects on scanning laser ophthalmoscope image quality of controlled amounts of scattered light, confocal pinhole diameter, and age. Optical volumes through the optic nerve head were recorded for a range of pinhole sizes in 12 subjects (19–64 years). The usefulness of various overall metrics in quantifying the changes in fundus image quality is assessed. For registered and averaged images, we calculated signal-to-noise ratio, entropy, and acutance. Entropy was best able to distinguish differing image quality. The optimum confocal pinhole diameter was found to be 50 μm (on the retina), providing improved axial resolution and image quality under all conditions.

OCIS codes: 110.2960, 110.3000, 170.1790, 170.3880, 330.4300, 330.4460.

1. INTRODUCTION

To help preserve vision, high quality fundus imaging is vital to early disease diagnosis and treatment monitoring. Ocular optical quality is degraded in the presence of ocular aberrations,[1,2] which are higher in some diseases,[3] in cataract,[4,5] and with age.[6] The amount of scattered light within the eye increases with age and in the presence of cataracts.[5,7–9] Both aberrations and scattered light will increase the axial and lateral volume in the wings of the point spread function (PSF) and reduce the central intensity compared with the diffraction-limited optical system. Moreover, the PSF will become asymmetric about the optical axis because of aberrations. All of these factors act to reduce both the quality of fundus images and the optical sectioning capability of a scanning laser ophthalmoscope (a microscope in which the objective lens is replaced by the optics of the eye).

Adaptive optics is an exciting new trend and a highly useful research technique in improved fundus imaging that corrects ocular aberrations. However, it cannot correct unwanted intraocular scattered light, and it is not yet available in a clinical instrument.[10]

The confocal scanning laser ophthalmoscope (CSLO, also called SLO)[11] is a clinically available instrument designed to minimize the effects of scattered light by means of a confocal pinhole (here referred to as the imaging pinhole) or limited detector area. The main application of a CSLO is clinical diagnosis of diseases that become more prevalent with increasing age. In particular, the ocular fundus of patients with cataracts, in whom scattered light is greatly increased, are able to be visualized with a CSLO,[12,13] whereas this is often difficult with traditional fundus cameras.[14]

A smaller confocal pinhole is expected to better control the effects of light scatter but potentially reduce the intensity response.[12,14] A large imaging pinhole or detector will also remove wide-angle scatter, greatly improving the contrast of images.[15] It has been shown that increased light scatter had little effect on contrast in a research CSLO image.[16] More recently Burke *et al.*[17] found no

significant effect of differing scatter-induced levels on the results from a commercial Heidelberg retinal tomograph, but the instrument's confocal pinhole was not defined. These previous measurements gave no insight into the optimum pinhole for best fundus images.

The theory behind the use of a confocal pinhole in a CSLO in relation to the PSF of the eye has previously been described.[18] With a very large confocal pinhole, the CSLO intensity is dependent on the PSF for light entering the eye. On the other hand, in an ideal CSLO, the confocal pinhole diameter is very small, and the image intensity is dependent on both the PSFs formed by ingoing and outgoing light. A small confocal pinhole will then reduce the impact of the intensity of light in the wings of the PSF and will maintain optical slicing capacity (axial resolution) but at the expense of intensity response.[14] As the pinhole size becomes larger, the intensity response improves, with a concurrent loss in axial resolution.[19]

CSLO axial and lateral resolutions have been predicted for a group of young subjects with the assumption of an infinitely small confocal pinhole.[20] Manivannan *et al.*[21] measured the expected axial resolution in a model eye in which the aberrations were not defined. The ideal pinhole for axial imaging in a diffraction-limited system is inadvisable for imaging the uncorrected eye because of the presence of aberrations that broaden the PSF. However, even in the absence of aberrations, pinholes, five times larger than ideal, improved microscope axial resolution.[22] In microscopy, the effect of the recommended[23] larger pinhole, needed for intensity response in the presence of aberrations,[19] on optical slicing has been investigated, but in scanning laser ophthalmoscopy in the human eye this effect is unknown and the pinhole sizes used are larger than recommended for microscopy[17,23]

To assess the impact of pinhole size on the quality of CSLO fundus images, optical quality metrics are needed. This image quality has traditionally been determined either in a subjective manner or by determining the signal-to-noise ratio (SNR).[24] The contrast across important image features, such as blood vessels, has also been used as a metric of image quality.[25–28] However, the measurement of vessel contrast is highly time consuming and involves subjective components. In the eye, acutance has been used previously to objectively quantify the clarity of the nerve fiber layer.[29]

In this work we will use different metrics to evaluate the quality of the fundus images recorded with a research CSLO as a function of pinhole size with changing age and induced scattered light. Images at differing optical depths were also obtained in order to assess the CSLO optical sectioning capability. We wish to determine which imaging pinhole size best balances intensity response and optical sectioning capability as a function of age.

2. METHODS

A. Experimental Setup and Procedure

Optic nerve head (ONH) images were acquired using a research CSLO ($\lambda = 632.8$ nm) shown in Fig. 1. A detailed description of the experimental system can be found elsewhere.[24] For this experiment, the CSLO was aligned to produce a square 15° field of view of the fundus. The

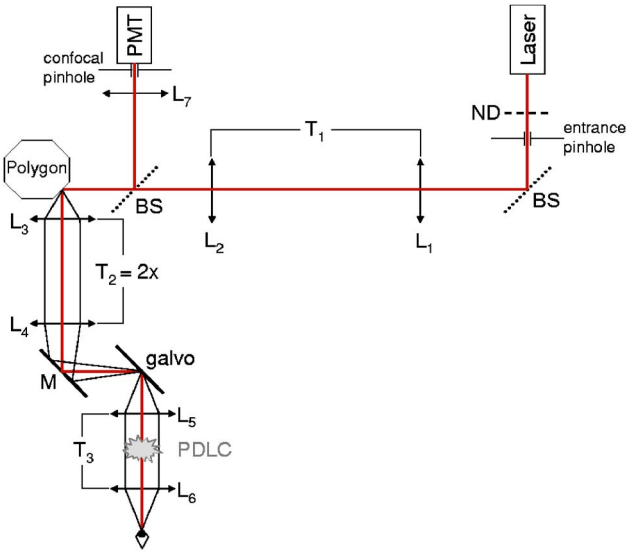

Fig. 1. (Color online) Schematic of the CSLO. Labels are as follows: ND, neutral density filter; BS, beam splitter; L, lenses; T, telescopes; M, mirror; galvo, galvanometer mirror; PDLC, scatter generator; PMT, photomultiplier tube.

resolution of each image was 512×512 pixels. For each person, sets of images were recorded for imaging pinhole diameters of 100, 200, 400, and 600 μm, approximately equivalent to 25, 50, 100, and 150 μm, respectively, on the fundus. A clear image of the nerve fiber layer surrounding the ONH corresponded to the 0 D reference focus. For each pinhole size, optical sections through the ONH on either side of this plane were obtained with the use of aberration-corrected trial lenses ranging in power from −1 D to +1 D in 0.5 D steps. Video segments, at a frame rate of 28.5 Hz, were recorded in sequence as the lenses in front of the eye were adjusted. Several seconds of streamed video were captured for each condition. The subject remained in their custom-made bite bar during the acquisition of each three-dimensional (3-D) volume. For each pinhole, the amount of light entering each eye was kept at a single level to optimize the real-time histograms of the CSLO images within the measured 3-D volume. This ensured that the images consisted of pixels of all intensities without saturation. With the smallest pinhole, the intensity required sometimes exceeded participant comfort levels and a lower level was used.

The CSLO was modified to include a scatter generator in the scanning path (Fig. 1), conjugate with the pupil of the eye and tilted slightly to remove any backreflections. The scatter generator is a polymer dispersed liquid-crystal (PDLC) cell consisting of micrometer size droplets of a dispersed liquid crystal (BL035 *MerckKgaA*) emulsified in a composite polymer (PN393 *MerckKgaA*) and sandwiched between two glass plates with transparent electrodes forming the gap (~10 μm thickness).[30,31] The refractive index for the polymer was 1.473 (for $\lambda = 589$ nm). For the birefringent liquid crystal, $n_{\text{ordinary}} = 1.528$ and $n_{\text{extraordinary}} = 1.473$, the same as for the polymer. Altering the AC voltage across the electrodes adjusts the transmission of the PDLC cell and generates different levels of scattered light. When no voltage is applied, the liquid crystals are randomly orientated. The refractive

index differences between the composite polymer and the liquid crystals result in light scattering and the cell appears cloudy. Once a voltage is applied, the liquid crystals begin to orient themselves and the difference in refractive indices reduces, thereby reducing the amount of light scattering and increasing the PDLC transparency. This PDLC cell follows Mie scattering theory, and it has previously been applied to simulate cataracts in measurements of visual acuity.[31] The relationship between the intensity of the scattered light and the voltage applied to the PDLC cell has been recently reported.[32] There was little scattered light for voltages larger than 2/3 of the maximum voltage (30 V), but it increased more rapidly across the lower range of voltages. For this lower range, as voltage decreased further, the scattered component of the light increased approximately linearly.

Video segments of the optical volume through the ONH were recorded without the PDLC cell and for differing degrees of scatter, produced by setting the voltage to the PDLC cell to its maximum value and to 9 V.[32] The lower amount of scatter (higher direct transmittance) produced at the maximum voltage setting is designated by $S=1.0$, and the larger amount of scatter (lower transmittance) at 9 V is designated by $S=0.2$. For a given pinhole, in the presence of the PDLC cell at a setting of 30 V, an increase in laser intensity of approximately 20% gave an intensity of light entering the eye equal to that in the absence of the PDLC cell. Thus, the normalized intensity, S, was set equal to 1.2 for CSLO images in the absence of the PDLC cell. Background images were recorded in each condition.

For each condition, an initial reference image was chosen. Using MATLAB (The MathWorks, Inc.), the seven frames with the highest correlation to this reference image were determined. The average of eight background frames was subtracted from each raw frame. The resulting eight images were registered (aligned and rotated to maximize their correlation) and averaged. For each subject, all averaged sections within a 3-D volume were then registered to allow accurate comparisons. For alignment, rotations of up to ±2° in 0.1° intervals and shifts of up to 35 pixels were automated. The resulting images are 412 $\times$ 412 pixels, corresponding to a 12° field. Occasionally, the software did not accurately rotate or align the slices sufficiently well. In these situations, the images were aligned by hand using PAINT SHOP PRO 9.

B. Participants

Twelve participants with normal ocular health were involved in this study. Their ages ranged from 19 to 64 years (39.5±4.7 years, mean±standard deviation) with two participants in each decade. The refractive errors of these participants ranged in sphere from +5.50 D to −7.25 D (mean sphere −1.5 D±1.0 D standard error). Their cylinders ranged from 0 D to −1.25 D (0.23 D±0.05 D). This research received ethics approval from the University of Waterloo Human Ethics Committee. All participants provided informed written consent. Light exposures were well below the maximum permissible exposures recommended by the American National Standards Institute (ANSI).[33] To induce pupil dilation and prevent accommodation, 1–2 drops of 0.5% tropicamide were instilled in one eye of each subject. The imaged eye varied among subjects and was chosen as the one with the lower refractive error and maximum visual acuity.

C. Image Quality Metrics

For each averaged image, SNR, Shannon entropy, and acutance were calculated. The intensity of each individual pixel, located at position (x,y) in the image, is given by $I(x,y)$. SNR is defined, as for speckle noise,[34] as the ratio of the mean $I(x,y)$ to the standard deviation of $I(x,y)$ across the entire image. A good quality image is expected to have a large SNR.

The second metric of image quality is Shannon entropy, a randomness measure that is defined (MATLAB 7.0.1) as

$$\text{Entropy} = -\sum_x \sum_y I(x,y)^2 \ln[I(x,y)^2].$$

This metric differs from traditional entropy,[35] calculated on the histogram. However, classical entropy and Shannon entropy were highly correlated across subjects ($R^2=0.96$). Shannon entropy will depend on the absolute values of the intensity levels. An image with a large number of bright pixels will have a high entropy value.

The third metric of image quality is acutance, an indicator of the intensity variations and the presence of features (such as nerve fiber layer structure) in the fundus images.[29,36]

$$\begin{aligned}\text{Acutance} = C\sum_x \sum_y [&|I(x,y) - I(x-1,y)|^2 + |I(x,y) - I(x+1,y)|^2 + |I(x,y) - I(x-1,y-1)|^2 + |I(x,y) - I(x+1,y-1)|^2 + |I(x,y) - I(x-1,y+1)|^2 + |I(x,y) - I(x+1,y+1)|^2 + |I(x,y) - I(x,y-1)|^2 + |I(x,y) - I(x,y+1)|^2].\end{aligned}$$

For these CSLO images, the constant[29] (C) is equal to 0.01487. Regardless of the gray level, the acutance of an image of constant intensity will be zero. Acutance is a metric of sharpness, and a good quality image with sharp features will be expected to have a high acutance.

Michelson contrast across a blood vessel was also determined for each participant.[25] The blood vessels chosen for analysis were oriented either horizontally or vertically.

D. Analysis Methods

Results among subjects and the impact of age, imaging pinhole diameter, focus plane, and scatter on the quality of fundus images were investigated using a repeated-measures analysis of covariance (RM-ANCOVA), with age as the covariate. This statistical test accounts for the expected within-subjects similarities while comparing the different imaging conditions. The sphericity assumption (that difference scores between any two levels of a factor do not depend on the levels analyzed) associated with a univariate analysis was tested. If it was violated ($p<0.05$), then the conservative Greenhouse–Geisser correction for the degrees of freedom was used, provided that epsilon was less than 0.75. Otherwise, the less conservative Huynh–Feldt correction was applied as recommended by Howell.[37] The multivariate test of significance, Wilks' lambda (Λ), which does not require the sphericity

assumption, was also used. Each metric's dependence on the experimental parameters was further visualized with functional fits. Pearson correlations and functional fits compared the image quality metrics used. To better understand the behavior of the image quality metrics, they were calculated as a function of the number of frames averaged up to a maximum of 16.

3. RESULTS

A. Effects of Frame Averaging

Averaging multiple image frames leads to improved image quality by reducing the effect of additive random noise.[38] However, as the number of averaged images increases, their alignment becomes more difficult, as multiple images are less well correlated. For SNR and entropy, the amounts of improvement observed as additional frames were included in an averaged image decreased (Fig. 2), as is also predicted theoretically for SNR in the presence of additive noise. We determined that the image quality improvement provided by averaging more than eight frames was not sufficient to warrant the increased computational complexity. Thus, for this study, the number of averaged images was eight. This is reflected in all future figures.

For a single series of averaged CSLO images, SNR and entropy increased in relation to the number of images in the average (Fig. 2). The actual improvement in SNR with frame averaging is slightly more rapid than the prediction from additive noise (Fig. 2, left). Conversely, although acutance is expected to increase with increasing image quality, it decreases as the number of averaged images increases (Fig. 2, right). This observed reduction in acutance with frame averaging is likely due to a reduction in speckle noise.

B. CSLO Imaging and Metric Repeatability

To test for repeatability, images for one young participant (age 29 years) were obtained under the same conditions at three different visits. Figure 3 shows averaged images obtained in the reference plane with the 400 μm pinhole. Subjectively, the first two visits appear more similar than the third visit. Cross-correlation coefficients among the images in Fig. 3 were 0.56, 0.30, and 0.35 for the first and second images, the first and third images, and the second and third images, respectively. Among single frames, consecutively recorded under identical conditions, cross-correlation coefficients above 0.8 were rare; usually much lower values were observed ($\sim$0.6).

To better examine these differences, the Fourier spectra for these images were calculated. Subtracting pairs of images gave differences among the Fourier spectra that were small and random. This implies that there were no systematic differences in images obtained on different occasions.

According to paired t-tests, across all conditions, SNR did not differ among the three visits. Acutance was only significantly ($p<0.02$) different between the first and the third visits. Entropy values differed ($p<0.04$) for the first and second visits and the second and third visits. According to Pearson correlation coefficients, SNR across depth, scatter, and pinhole size was not well correlated ($R<0.6$) across visits. Entropy and acutance had higher correlation values ($0.68<R<0.88$) across visits.

Imaging for a second participant (age 30 years) was also repeated on two different days. For this participant, each metric across depth, scatter, and pinhole size was well correlated between the two visits ($R>0.90$); but paired t-tests indicate that SNR, entropy, and acutance were each significantly ($p<0.001$) different.

C. Image Quality Metrics: Detailed Analysis for a Sample Participant

Figure 4 (top row) shows a through-focus series of CSLO images obtained using a 400 μm imaging pinhole with no induced scatter in the 29 year old participant. The upper blood vessels are in focus in the presence of a 1 D lens. As

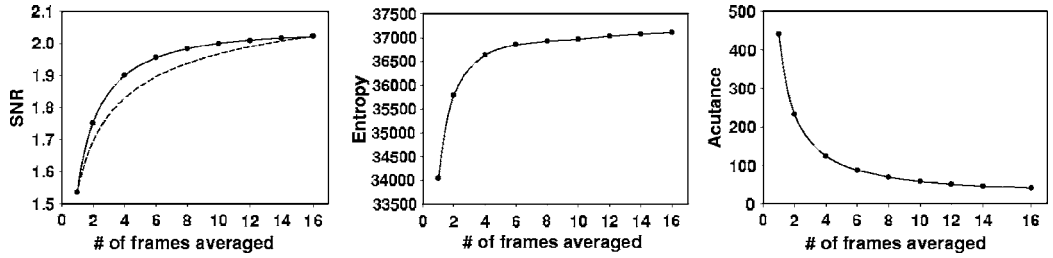

Fig. 2. Image quality metrics plotted as a function of the number of image frames averaged for the 29 year old participant. The solid curve represents the best fit regression. For SNR, the predicted rate of change for additive noise is also shown (dashed curve).

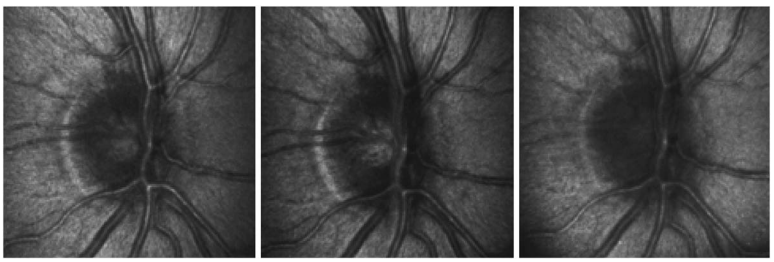

Fig. 3. Averaged CSLO images obtained for a 29 year old participant with the 400 μm pinhole at the reference plane (0 D) with no induced scatter on three different occasions.

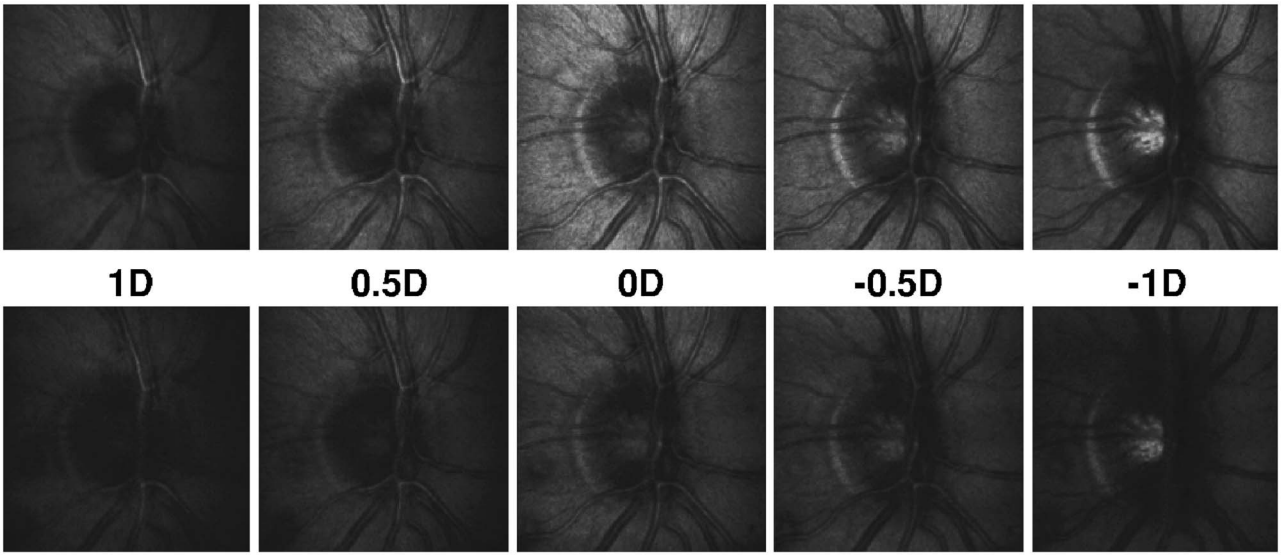

Fig. 4. Series of through-focus CSLO images using a 400 μm imaging pinhole for a 29 year old participant. The top row of images was obtained with no induced scatter. A scattering device ($S=0.2$) was placed conjugate to the entrance pupil of the eye during the acquisition of images in the bottom row.

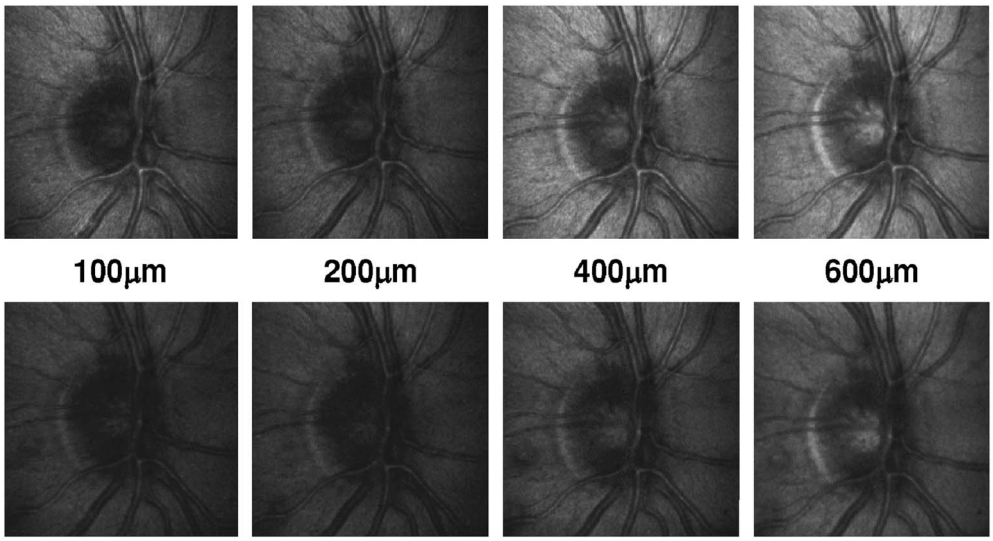

Fig. 5. CSLO images (0 D) of a 29 year old participant with varying imaging pinhole diameters with no induced scatter (top row) and in the presence of a scatter level $S=0.2$ (bottom row). The small circles on the left side of the images with induced scatter are artifacts from the PDLC cell.

the lens power decreases, the retinal nerve fiber layer, lower blood vessels, neural retinal rim, and the cup edge of the ONH come into focus. With deeper optical sections, the lamina cribrosa and its pores become visible. The presence of scattered light (Fig. 4, bottom row) reduced image brightness and resulted in a subjective degradation of image quality for this pinhole diameter. The differences in the images with lens power were visible in their Fourier spectra, but there are no obvious differences among the Fourier spectra for different pinholes. Subjective image quality also varied with imaging pinhole diameter (Fig. 5, top row). These images were also degraded by the presence of induced scatter (Fig. 5, bottom row).

The metrics were used to objectively quantify the observed changes in image quality with different lenses, pinholes, and scatter levels. First, each metric was plotted versus the lens power used in the optical sectioning for the four different imaging pinhole diameters in the absence of any induced scattered light (Fig. 6). According to all three metrics, image quality differed with imaging pinhole diameter and the position of optical focus (lens). There was a peak in entropy at the reference plane (0 D). SNR and entropy suggest that a larger pinhole gives better image quality. For all three metrics, the 100 and 200 μm pinholes had poorer overall image quality metric values than larger sized pinholes. Similar plots of ONH vessel contrast values versus lens power did not show clear trends. Entropy and acutance showed similar trends with acutance increasing with increasing subjective image quality (Fig. 6). This is opposite to the result with

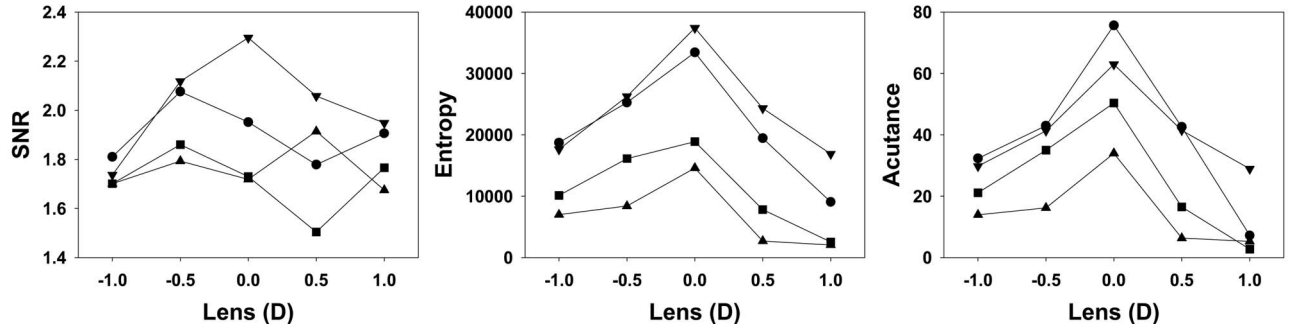

Fig. 6. For no induced scatter, each of the three metrics for a 29 year old participant was plotted versus the lens power used for optical sectioning with four different imaging pinhole diameters. Squares, 100 μm; upright triangles, 200 μm; circles, 400 μm; downward triangles, 600 μm.

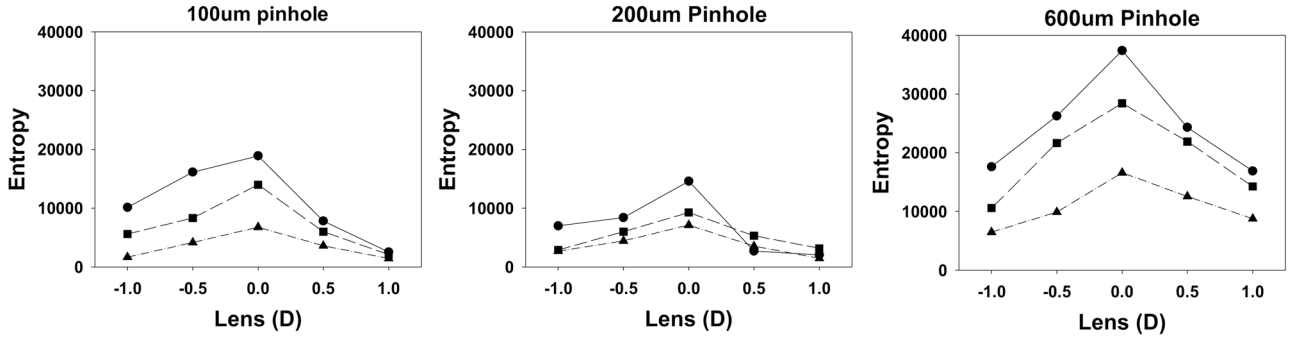

Fig. 7. (Color online) For the 100, 200, and 600 μm imaging pinholes, entropy (shown on the same scale) for a 29 year old participant was plotted versus the lens power used in the optical sectioning for varying amounts of scattered light. Triangles, $S=0.2$; squares, $S=1.0$; circles, $S=1.2$.

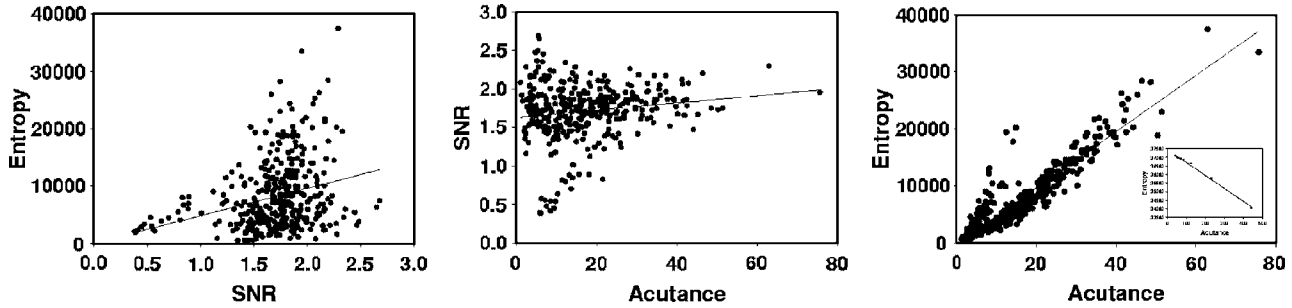

Fig. 8. Scatterplots comparing SNR, entropy, and acutance for all imaging conditions. Lines are significant linear regressions. The insert in the plot of entropy versus acutance shows the negative correlation for the metrics calculated for images with different numbers of averaged frames.

frame averaging (Fig. 2), where acutance decreased with increasing numbers of frames averaged, which gave a subjective improvement. Because of these results, additional acutance plots for this subject will not be shown.

In comparing the averaged images, the smaller imaging pinholes have better optical sectioning capabilities, as can be seen by the absence of a visible lamina cribrosa with the 100 and 200 μm pinholes for the reference imaging plane in Fig. 5 (top row). Therefore the apparent improvement in image quality metrics at larger pinhole sizes may be due to the increased visibility of additional structures with the loss of optical sectioning.

The image metric values were plotted versus the lens power used in the optical sectioning for the different amounts of induced scattered light, including no induced scatter, for the 400 μm imaging pinhole diameter (not shown). SNR did not quantify the reduction in image quality due to induced scatter, noticeable in the actual images. On the other hand, both entropy and acutance quantified degradation in image quality with increasing scattered light.

To examine the effect of scatter on image quality for different pinhole diameters (Fig. 5, bottom), entropy was plotted versus lens power for different amounts of scattered light across the different pinhole diameters (Fig. 7). The curves were closer together with the smaller pinholes than for the larger pinhole diameters. Hence, there is less reduction in quality with scatter for a smaller pinhole.

D. Correlations Among Metrics across Subjects

The three image quality metrics are expected to measure different image properties. Pearson correlation coeffi-

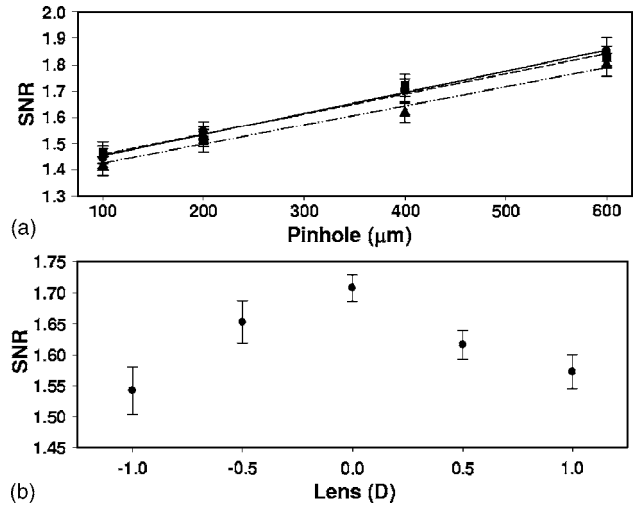

Fig. 9. (a) SNR versus pinhole for the three different levels of scatter. Each point is the average across all eyes and lenses for each pinhole and scatter setting. Error bars represent the standard error. The circles and solid line represent the absence of induced scatter. The squares (with dashed line) and triangles (with dashed–dotted line) represent the presence of increasing induced scatter at the 1.0 and 0.2 PDLC settings, respectively. (b) SNR plotted versus lens power (D) used in the optical sectioning. Each point is the average across all eyes, pinholes, and scatter settings for each lens. Error bars represent the standard error.

cients were determined among SNR, entropy, and acutance for all of the image conditions analyzed across subjects. In the case of measurements repeated on the same subject on several different days, only the first set of data was included. All correlations were significant ($p \leq 0.001$) and are shown in Fig. 8. SNR was poorly correlated with entropy ($R=0.439$) and acutance ($R=0.378$). Even though they differ mathematically, entropy and acutance were very highly correlated ($R=0.940$). This result differs from the change in metrics with frame averaging, where entropy and acutance were negatively correlated. Because of this unexpected result, the values of acutance for varying pinholes and scatter will not be shown in detail.

Neither vessel central contrast ($R=0$) nor edge contrast ($R<0.15$) was well correlated with any of the image quality metrics. Linear regressions were successful between edge contrast and both entropy and acutance; however, the fits were weak ($R^2<0.1$).

E. Image Quality Metrics across Subjects and Conditions

1. Signal-to-Noise Ratio

According to a RM-ANCOVA on the SNR values, there is a significant interaction between imaging pinhole diameter and light scatter ($\Lambda=0.126$, $p=0.037$). A plot of SNR versus pinhole for the three different levels of scatter is shown in Fig. 9(a). For each separate level of scatter, SNR increased linearly with pinhole diameter with near parallel slopes. The RM-ANCOVA is sensitive to the small in-

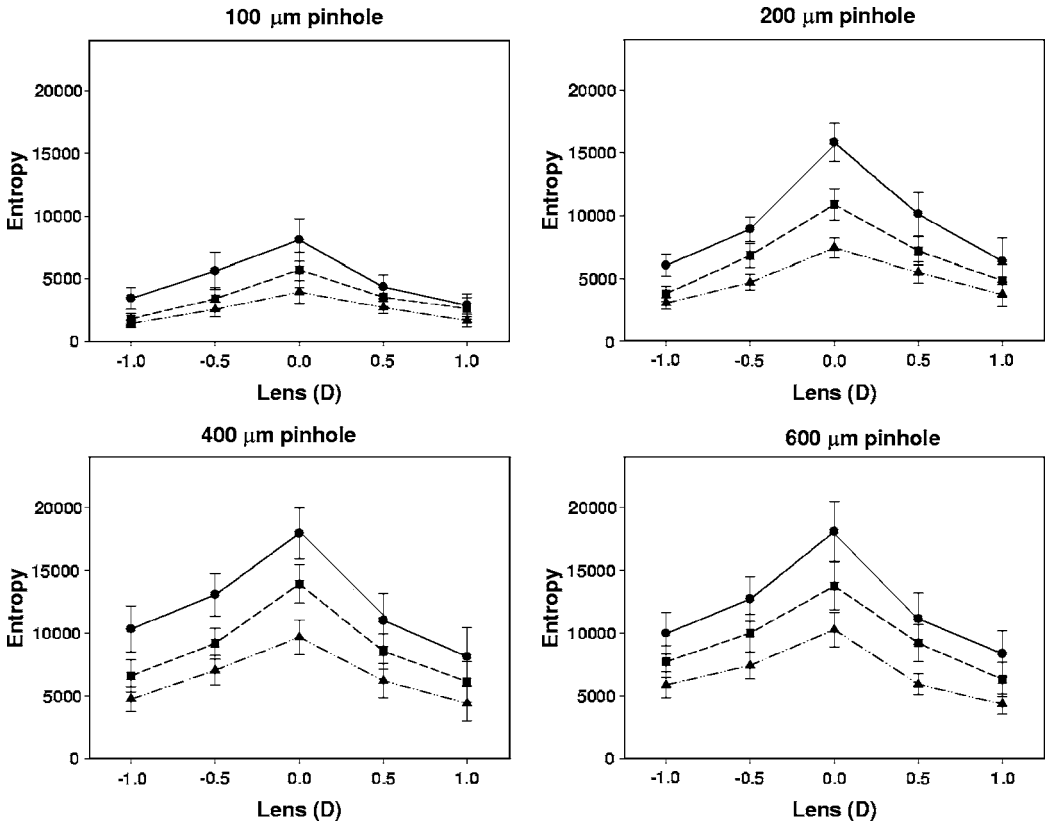

Fig. 10. Entropy versus lens power for the three different scatter conditions, with separate graphs for each imaging pinhole diameter. Each point is the average across all eyes for each imaging condition. Error bars represent the standard error. The circles and solid curve represent the absence of induced scatter. The squares (with dashed curve) and triangles (with dashed-dotted curve) represent the presence of increasing induced scatter at the 1.0 and 0.2 PDLC settings, respectively.

crease in the intercept of the curves with decreasing amounts of scatter. The differences with pinhole size are larger than the differences with scatter. As with the results for the sample 29 year old participant previously discussed, the improvement in SNR with increasing pinhole may be confounded by the concurrent reduction in optical sectioning capability. Overall, according to the RM-ANCOVA, lens power did not significantly affect the SNR [Fig. 9(b)].

2. Entropy

For entropy, there is a significant (RM-ANCOVA, sphericity assumed, $p=0.019$) interaction among pinhole, lens, and scatter. To better understand this interaction, the entropy averaged across subjects was plotted versus lens, with separate curves for the different levels of scatter and differing pinhole sizes (Fig. 10). Scatter reduced quality over all pinholes. As was found in the detailed analysis of the single participant, with a smaller pinhole there is less reduction in quality with scatter than with a larger pinhole. Across all pinholes, entropy drops by similar percentages (approximately 50%) from the value in the absence of scatter ($S=1.2$) to the value in the presence of the largest amount of scatter ($S=0.2$). Across all lenses for all levels of scatter, the entropy values for the 400 and 600 μm pinholes were very similar. The image quality with the 200 μm pinhole was only slightly worse. However, unlike for the 29 year old participant, the overall image quality across subjects for all levels of scatter was noticeably reduced with the smallest pinhole.

3. Acutance

From the RM-ANCOVA, acutance was significantly impacted by the position of focus (lens) and by induced scatter in a manner similar to entropy. On the other hand, no significant effects with varying imaging pinholes or participant age were suggested by the RM-ANCOVA. However, acutance increased exponentially with imaging pinhole diameter.

F. Effect of Age on Image Quality

For this initial sample size, none of the metrics found a significant effect of age on the quality of the CSLO images. Plots of the metric means, averaged across all conditions, as a function of age are shown in Fig. 11. No clear trends with age are visible. There appears to be no clustering of any metrics due to refractive error or gender. Exclusion of the images obtained in the presence of induced scatter does not reveal any masked relationships.

Subjectively, image quality appears to worsen with age at smaller imaging pinholes. To test this hypothesis, the image quality metrics were plotted versus age for each pinhole diameter for images obtained with differing levels of induced scattered light. This is appropriate because, according to entropy, there is a significant interaction among pinhole, lens, and scatter. Entropy linearly decreased with age for all scatter levels (Fig. 12) for a 100 μm pinhole ($0.37 \leqslant R^2 \leqslant 0.53$). For the different levels of scatter, the slopes did not differ, but the intercept dropped as the amount of induced scatter increased, indicating that, although there appears to be significant scatter reduction with this small pinhole, there is still some residual effect of scatter. Acutance decreased significantly ($R^2 \leqslant 0.53$) with age for only the largest induced scatter level. At no other pinhole diameter, for any scatter level, did any of the three metrics change significantly with age.

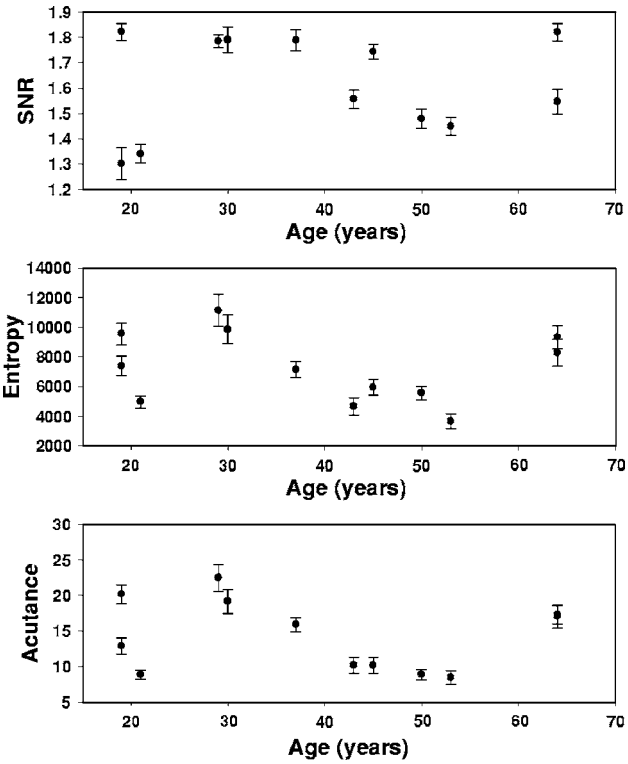

Fig. 11. Image quality metrics as a function of age. Each point is the average across all pinholes, lenses, and scatter settings for each eye. Error bars represent the standard error.

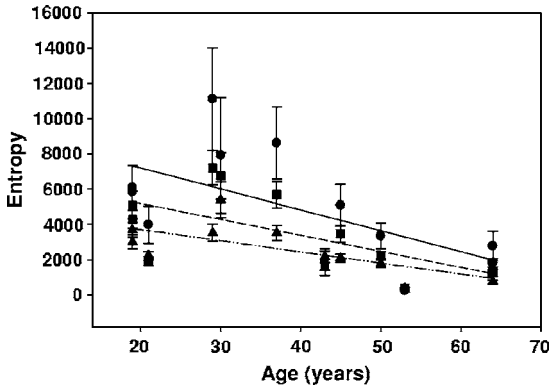

Fig. 12. Entropy plotted versus age for the 100 μm imaging pinhole in the absence of induced scatter (circles) and for two scatter settings (squares, $S=1.0$; triangles, $S=0.2$). The lines represent the significant linear regressions.

4. DISCUSSION

A. Repeatability of Imaging and Metrics

CSLO measurements were fairly repeatable within a subject. Entropy and acutance were more repeatable than the CSLO image cross correlations among visits. SNR was not as repeatable.

B. Image Quality Metrics

We are interested in which image quality metrics can differentiate image quality changes with age, the amount of

induced scatter, confocal pinhole size, the position of focus of the CSLO, and in interactions among these variables. Induced scatter and the reduction of noise with increasing frame averaging are the two variables for which image quality variation is known. There is an unambiguous degradation in quality with increasing scatter and an improvement in quality with increasing frame averaging. As expected, entropy and SNR improved with frame averaging and deteriorated with increased scatter. However, acutance decreased with increasing numbers of averaged frames (a negative correlation with entropy), but it increased with retinal images that had lower scatter and subjectively improved sharpness (a positive correlation with entropy). Thus, caution should be exercised when interpreting acutance values for different CSLO images. Although significantly affected by lens power, scatter, and pinhole size and correlated among visits, acutance found no significant interactions among the changing imaging conditions. Nonetheless, acutance may be useful for quantifying image quality in restricted fundus regions that contain only a select feature such as the nerve fiber layer.[29]

SNR identified a significant interaction between pinhole diameter and induced scatter but did not identify the effects of either age or focal plane, which are subjectively visible. However, SNR can give information on the behavior of noise in CSLO images.

Entropy was well correlated within a participant on different visits; identified an interaction among pinhole, lens, and scatter in overall fundus image quality; and revealed linear reductions in image quality with increasing age for the 100 μm imaging pinhole diameter for each level of scatter. Broadly, the results of all metrics were consistent, but entropy of a CSLO image appears most consistent and sensitive for monitoring the overall quality of fundus images.

SNR, entropy, and acutance are measures of global image quality, while the contrast across a blood vessel is a local measure of image quality and may vary depending on the location and type of the blood vessel chosen for analysis. Acutance and entropy were both only weakly linearly correlated with the blood vessel edge contrast, perhaps because of the differing vessel positions. Thus, these global image quality metrics provide information additional to that of blood vessel contrast.

C. Image Quality and Pinhole Size

The imaging pinholes used in this experiment, projected onto the fundus of an emmetropic schematic eye, are approximately equal to 25, 50, 100, and 150 μm in diameter. This is at least five times larger than the ideal pinhole diameter suggested by Wilson and Carlini[39] for optimum axial resolution for a diffraction-limited PSF. Booth *et al.*[19] recommend a pinhole size that captures 50% of the integrated lateral aberrated PSF intensity in the presence of aberrations. For a symmetric Gaussian approximation of the PSF, 50% of the integrated intensity due to aberrations occurs at approximately the half-height of the lateral PSF. For a 3.3 mm pupil, the actual, aberrated PSF in the eye is approximately 1.4 arcmin in diameter at the half-height,[40] or smaller.[41] For a 6.6 mm pupil, more similar to the outgoing dilated pupil in this experiment, the full width at half-height is approximately 2 arcmin,[40] or up to 4 arcmin.[2] This larger value gives a corresponding ideal pinhole of ~20 μm for a mostly young population. Higher-order aberrations vary across individuals[1,2,40,42] and with age,[6] and the lateral PSF increases in diameter by a factor of approximately 1.6 from age 20–30 years to age 60–70 years,[6] giving a PSF with double-pass dimensions for a 4 mm pupil[43] closer to those of the smallest pinhole used in this experiment. Therefore, the imaging pinholes in this experiment were expected primarily to remove wide-angle scatter and potentially improve depth resolution.

1. Axial Resolution and Optical Sectioning

The image quality metrics varied with the different positions of focus in depth [Figs. 6, 7, 9(b), and 10]. Features in focus changed with the lens power in front of the eye, indicating the presence of some degree of optical sectioning, even with the largest imaging pinhole used (Figs. 4, 7, and 10).

Each optical section is located approximately 180–190 μm from adjacent sections within the 3-D volume (assuming a 60 D schematic eye with a retinal refractive index of 1.336). Donnelley and Roorda[20] predicted an axial resolution of approximately 200 μm for a 3.3 mm pupil diameter in an aberrated eye (with equal ingoing and outgoing beam diameters) for an ideal pinhole. Thus, the axial thickness corresponding to the lens differences in two adjacent images is close to the expected axial resolution in the ideal confocal pinhole case. Hence, particularly with the larger imaging pinholes, it is expected that there will be light from out of plane structures accepted by the pinhole, making them visible in more than one axial plane. This was subjectively observed experimentally since optical sectioning appears better defined for the two smaller imaging pinholes and worsens at the two larger pinholes. For this data set, the 100 and 200 μm imaging pinholes provide similar and best axial sectioning capabilities. The experimentally observed optical sectioning and the full widths at half-height of entropy plotted versus lens power (Fig. 10) suggest an axial resolution of approximately 250 μm for the two smallest imaging pinhole diameters. This is better than the intensity response predicted for an uncorrected larger pupil but much worse than an adaptive optics corrected eye.[44] Quantification of entropy for a specific localized region, such as a single feature in the lamina cribrosa or a thin blood vessel, may be more appropriate for determining the intensity response capabilities for each pinhole. Images at intermediate focal planes might allow use of a plot of entropy versus lens power to define the axial resolution under differing conditions.

2. Image Quality within an Optical Section

As previously stated, the image quality metrics are not able to distinguish whether increases in intensity originate from in-focus or out-of-focus planes. SNR linearly increased with imaging pinhole diameter. For entropy and acutance, some individual participants (such as the 29 year old participant) showed better quality for a 100 μm pinhole compared with a 200 μm imaging pinhole, while most had better quality at larger pinholes.

Central blood vessel contrast was better with the smaller pinholes as compared with the two larger pinholes, in agreement with the subjective impression of image contrast. The eye's PSFs due to aberrations are likely smaller than the imaging pinhole diameters projected onto the retina. However, scattered light spreads the PSF more than aberrations do. It is possible that the smaller imaging pinhole is excluding more scattered light than are the larger pinholes, leading to the improved contrast observed.

D. Image Quality and Scattered Light

Both SNR and entropy quantified the negative effects of induced light scatter on overall image quality (Figs. 7 and 10). In the presence of the scatter generator, intensity entering the eye and thus the volume under the eye's PSF were kept constant for a given pinhole diameter. Subjectively, image brightness was reduced in the presence of scattered light (Figs. 4 and 5), presumably because more of the scattered light was excluded by the imaging pinholes. There was less absolute impact of induced scatter on image quality in the presence of the smaller confocal pinholes for the individual subject analyzed (Fig. 7) and across subjects (Fig. 10). This implies that the smaller pinhole may better negate the effect of increased light scatter. This is consistent with the expected performance of a SLO[15] or CSLO.[18] However, the effect of scattered light is still measurable (Figs. 7, 10, and 12). This implies that some of the induced light scatter is at moderate angles and is not excluded by even the smallest imaging pinholes. In the presence of induced scattered light, the flattening of plots of entropy versus lens power (Fig. 10) is also suggestive of reduced axial sectioning capabilities.

E. Participant Age and Fundus Image Quality

Surprisingly, when all factors were considered together (or in the absence of induced scatter), there were no significant changes in overall image quality or ONH vessel contrast with age. With the natural increase in higher-order aberrations and light scatter during aging, the PSF will drop in peak intensity and have a larger spread. As such, image quality and axial sectioning are expected to degrade with age because of their dependence on the ingoing PSF and the outgoing scattered light.

The reduction in image quality with age, expected due to an increase in the spread of the PSF (in the absence of induced scattered light), was apparent only at the smallest pinhole diameter according to entropy. The intensity of light going into the eye was adjusted for each person in an attempt to optimize the CSLO image histogram. For all participants, the smaller the imaging pinhole, the larger the amount of light needed to optimize the histogram. On average, at a given pinhole diameter, a higher intensity of light was required for the older subjects as compared with the younger subjects, consistent with an increase in light scatter with age. However, with the 100 μm imaging pinhole, the light required to optimize the histogram in many of the older subjects was above their comfort level, even in the absence of induced light scatter. Hence, the reduction in image quality with age for the 100 μm imaging pinhole may have been in part a consequence of reduced light returning to the detector. In addition, a larger pinhole at older ages may be necessary to capture the 50% of the lateral PSF intensity recommended by Booth *et al.*[19]

The lack of an effect of age at larger pinholes suggests that older subjects can obtain images comparable in quality, as quantified by the metrics applied here, to those of younger eyes. Alternatively, it may be the result of a lack of sample power. To show an effect of age on entropy and acutance between those younger than 30 years old and those older than 60 years, 27 participants would be required in each group.

F. Optimum Choice of Imaging Pinhole

Subjectively, the 100 and 200 μm imaging pinholes both provide better optical sectioning than do the larger pinholes. All pinholes reduce some, but not all, effects of induced scattered light. With age, image quality was reduced only with the 100 μm imaging pinhole. Therefore, for a given optical focus across all subjects, the 200 μm imaging pinhole ($\sim$50 μm on the retina) provided the best image quality. However, for some subjects, the 100 μm pinhole ($\sim$25 μm on the retina) was better.

If even smaller imaging pinholes with potentially better optical sectioning capability are desired, the use of a longer wavelength would allow more light to enter the eye at a comfortable level. The effect of altering pinhole size to capture varying amounts of the integrated lateral PSF intensity[19] could then be explored at smaller pinholes.

5. CONCLUSIONS

The image quality metrics, SNR, entropy, and acutance, objectively quantify more global aspects of fundus images than does blood vessel contrast. Entropy appears to be the most useful metric for quantifying differences in fundus image quality. It varied monotonically as expected for averaged images and induced scatter; was well correlated within a participant on different occasions; identified a significant interaction among pinhole, focal plane, and induced scatter; and showed a reduction in quality with age at the smallest pinhole. However, the image quality metrics are affected by the increase in image intensity at larger imaging pinholes resulting from reductions in axial sectioning capability. With more focal plane samples, the half-width of entropy as a function of focal position (lens power) may provide a quantification of optical sectioning capability. For an aberrated eye, pinhole size affects image quality, contrast, and optical sectioning even for pinhole sizes much larger than the aberrated PSF. Moderately sized imaging pinholes of 100 or 200 μm ($\sim$25 and 50 μm on the retina) provided improved optical sectioning capabilities and good image quality and contrast over a range of ages. For the red light used here, the optimum imaging pinhole diameter across all participants under all conditions was 200 μm ($\sim$50 μm on the retina). It provided good optical sectioning ability with high values across a range of ages for the image quality metrics and ONH vessel contrast. This pinhole size also reduced the effects of varying amounts of scattered light induced artificially with a PDLC cell, so it is expected to be a good choice when imaging subjects with excess scattered light due to cataracts.

ACKNOWLEDGMENTS

The authors thank L. Epps for his assistance with data analysis. This research was supported by the Ontario Centre for Excellence, Centre for Photonics, NSERC Canada, and an Ontario Graduate Scholarship to Jennifer J. Hunter.

Corresponding author Melanie C. W. Campbell can be reached by e-mail at mcampbel@sciborg.uwaterloo.ca.

*Present address, Center for Visual Science, University of Rochester, Rochester, New York 14627–0270, USA.

REFERENCES

1. J. Liang and D. R. Williams, "Aberrations and retinal image quality of the normal human eye," J. Opt. Soc. Am. A **14**, 2873–2883 (1997).
2. L. N. Thibos, X. Hong, A. Bradley, and X. Cheng, "Statistical variation of aberration structure and image quality in a normal population of healthy eyes," J. Opt. Soc. Am. A **19**, 2329–2348 (2002).
3. M. Shahidi, N. P. Blair, M. Mori, and R. Zelkha, "Optical section retinal imaging and wavefront sensing in diabetes," Optom. Vision Sci. **81**, 778–784 (2004).
4. T. Kuroda, T. Fujikado, N. Maeda, T. Oshika, Y. Hirohara, and T. Mihashi, "Wavefront analysis in eyes with nuclear or cortical cataract," Am. J. Ophthalmol. **134**, 1–9 (2002).
5. P. W. de Waard, J. K. Ijspeert, T. J. van den Berg, and P. T. de Jong, "Intraocular light scattering in age-related cataracts," Invest. Ophthalmol. Visual Sci. **33**, 618–625 (1992).
6. P. Artal, A. Guirao, E. Berrio, P. Piers, and S. Norrby, "Optical aberrations and the aging eye," Invest. Ophthalmol. Visual Sci. **43**, 63–77 (2003).
7. T. Kuroda, T. Fujikado, S. Ninomiya, N. Maeda, Y. Hirohara, and T. Mihashi, "Effect of aging on ocular light scatter and higher order aberrations," J. Refract. Surg. **18**, S598–602 (2002).
8. J. K. Ijspeert, P. W. de Waard, T. J. van den Berg, and P. T. de Jong, "The intraocular straylight function in 129 healthy volunteers: dependence on angle, age and pigmentation," Vision Res. **30**, 699–707 (1990).
9. G. Westheimer and J. Liang, "Evaluating diffusion of light in the eye by objective means," Invest. Ophthalmol. Visual Sci. **35**, 2652–2657 (1994).
10. Y. Zhang, S. Poonja, and A. Roorda, "MEMS-based adaptive optics scanning laser ophthalmoscopy," Opt. Lett. **31**, 1268–1270 (2006).
11. R. H. Webb, G. W. Hughes, and O. Pomerantzeff, "Flying spot TV ophthalmoscope," Appl. Opt. **19**, 2991–2997 (1980).
12. C. Beckman, L. Bond-Taylor, B. Lindblom, and J. Sjostrand, "Confocal fundus imaging with a scanning laser ophthalmoscope in eyes with cataract," Br. J. Ophthamol. **79**, 900–904 (1995).
13. L. Zangwill, I. Irak, C. Berry, and V. Garden, "Effect of cararact and pupil size on image quality with confocal scanning laser ophthalmoscopy," Arch. Ophthalmol. (Chicago) **115**, 983–990 (1997).
14. A. Plesch, U. Klingbeil, W. Rappl, and C. Schrodel, "Scanning ophthalmic imaging," in *Scanning Laser Ophthalmoscopy and Tomography*, J. E. Nasemann and R. O. W. Burk, eds. (Quintessenz, 1990), pp. 23–33.
15. R. H. Webb and G. W. Hughes, "Scanning laser ophthalmoscope," IEEE Trans. Biomed. Eng. **BME28**, 488–492 (1981).
16. C. Beckman, M. Atkinson, M. Stargard, R. Munger, and M. Campbell, "The influence of increased interocular light scatter on the contrast in a confocal scanning laser ophthalmoscope image," in *Vision Science and its Applications*, Vol. 1 of 1995 OSA Technical Digest Series (Optical Society of America, 1995), pp. 55–69.
17. M. A. Burke, C. J. Khanna, A. Miller, S. T. Venkataraman, and C. Hudson, "The impact of artificial light scatter on scanning laser tomography," Optom. Vision Sci. **83**, 222–227 (2006).
18. A. J. Roorda, "Double pass reflections in the human eye," Ph.D. thesis (University of Waterloo, Canada, 1996).
19. M. J. Booth, M. A. A. Neil, and T. Wilson, "Aberration correction for confocal imaging in refractive-index-mismatched media," J. Microsc. **192**, 90–98 (1998).
20. W. J. Donnelly III and A. Roorda, "Optimal pupil size in the human eye for axial resolution," J. Opt. Soc. Am. A **20**, 2010–2015 (2003).
21. A. Manivannan, P. F. Sharp, and J. V. Forrester, "Performance-measurements of an infrared digital scanning laser ophthalmoscope," Physiol. Meas. **15**, 317–324 (1994).
22. T. Wilson, "The role of the pinhole in confocal imaging system," in *Handbook of Biological Confocal Microscopy*, J. B. Pawley, ed. (Plenum, 1995), pp. 167–182.
23. M. J. Booth, M. A. A. Neil, R. Juskaitis, and T. Wilson, "Adaptive aberration correction in a confocal microscope," Proc. Natl. Acad. Sci. U.S.A. **99**, 5788–5792 (2002).
24. J. M. Bueno and M. C. W. Campbell, "Confocal scanning laser ophthalmoscopy improvement by use of Mueller-matrix polarimetry," Opt. Lett. **27**, 830–832 (2002).
25. K. Muth, M. C. W. Campbell, A. J. Roorda, and C. Cui, "The effect of entrance beam location on image quality of CSLO images," in *Vision Science and Its Applications*, Vol. 1 of 1997 OSA Technical Digest Series(Optical Society of America, 1997), pp. 56–59.
26. K. M. Muth, "The effect of entrance beam diameter and position within the pupil on the image quality of a confocal scanning laser ophthalmoscope," MSc thesis (University of Waterloo, Canada, 1998).
27. J. M. Bueno and B. Vohnsen, "Polarimetric high-resolution confocal scanning laser ophthalmoscope," Vision Res. **45**, 3526–3534 (2005).
28. S. A. Burns, A. E. Elsner, M. B. Mellem-Kairala, and R. B. Simmons, "Improved contrast of subretinal structures using polarization analysis," Invest. Ophthalmol. Visual Sci. **44**, 4061–4068 (2003).
29. Y. F. Choong, F. Rakebrandt, R. V. North, and J. E. Morgan, "Acutance, an objective measure of retinal nerve fibre image clarity," Br. J. Ophthamol. **87**, 322–326 (2003).
30. S. J. Cox, V. Y. Reshetnyak, and T. J. Sluckin, "Theory of dielectric and optical properties of PDLC films," Mol. Cryst. Liq. Cryst. **320**, 301–320 (1998).
31. M. Ozolinsh and G. Papelba, "Eye cataract simulation using polymer dispersed liquid crystal scattering obstacles," Ferroelectrics **304**, 1037–1042/207–212 (2004).
32. J. M. Bueno, E. Berrio, M. Ozolinsh, and G. Ikaunieks, "Optical properties of a polymer dispersed liquid crystal to be used on visual testing," in *Proceedings of ICO Topical Meeting on Optoinformatics/Information Photonics* (ICO, 2006), pp. 276–278.
33. American National Standards Institute, "American National Standard for safe use of lasers," Z136.1-2000 (Laser Institute of America, 2000).
34. J.W. Goodman, "Statistical properties of laser speckle patterns," in *Topics in Applied Physics: Laser Speckle and Related Phenomena*, J. C. Dainty, ed. (Springer-Verlag, 1975), Vol. 9, pp. 9–75.
35. R. C. Gonzalez, R. E. Woods, and S. L. Eddins, *Digital Image Processing Using MATLAB* (Pearson Prentice Hall, 2004), p. 609.
36. R. M. Rangayyan, N. M. El-Faramawy, J. E. Desautels, and O. A. Alim, "Measures of acutance and shape for classification of breast tumors," IEEE Trans. Med. Imaging **16**, 799–810 (1997).
37. D. C. Howell, *Statistical Methods for Psychology* (Duxbury/Thomson Learning, 2002).
38. K. R. Castleman, *Digital Image Processing* (Prentice Hall, 1996).
39. T. Wilson and A. R. Carlini, "Size of the detector in confocal imaging systems," Opt. Lett. **12**, 227–229 (1987).
40. F. W. Campbell and R. W. Gubisch, "Optical quality of the human eye," J. Physiol. (London) **186**, 558–578 (1966).

41. J. Liang and G. Westheimer, "Optical performances of human eyes derived from double-pass measurements," J. Opt. Soc. Am. A **12**, 1411–1416 (1995).
42. P. Artal and R. Navarro, "Monochromatic modulation transfer function of the human eye for different pupil diameters: an analytical expression," J. Opt. Soc. Am. A **11**, 246–249 (1994).
43. P. Artal, M. Ferro, I. Miranda, and R. Navarro, "Effects of aging in retinal image quality," J. Opt. Soc. Am. A **10**, 1656–1662 (1993).
44. K. Venkateswaran, A. Roorda, and F. Romero-Borja, "Theoretical modeling and evaluation of the axial resolution of the adaptive optics scanning laser ophthalmoscope," J. Biomed. Opt. **9**, 132–138 (2004).